

# A Macroporous Hydrogel Dressing with Enhanced Antibacterial and Anti-Inflammatory Capabilities for Accelerated Wound Healing

Wen-Can Huang, Rui Ying, Wei Wang, Yuning Guo, Yongjun He, Xinya Mo, Changhu Xue,\* and Xiangzhao Mao\*

Here, a novel macroporous hydrogel dressing is presented that can accelerate wound healing and guard against bacteria-associated wound infection. Carboxymethyl agarose (CMA) is successfully prepared from agarose. The CMA molecular chains are cross-linked by hydrogen bonding to form a supra-molecular hydrogel, and the hydroxy groups in the CMA molecules complex with  $\text{Ag}^+$  to promote hydrogel formation. This hydrogel composite exhibits pH-responsiveness and temperature-responsiveness and releases  $\text{Ag}^+$ , an antibacterial agent, over a prolonged period of time. Moreover, this hydrogel exhibits outstanding cytocompatibility and hemocompatibility. In vitro and in vivo investigations demonstrate that the hydrogel has enhanced antibacterial and anti-inflammatory capabilities and can significantly accelerate skin tissue regeneration and wound closure. Astonishingly, the hydrogel can cause the inflammation process to occur earlier and for a shorter amount of time than in a normal process. Given its excellent antibacterial, anti-inflammatory, and physicochemical properties, the broad application of this hydrogel in bacteria-associated wound management is anticipated.

Having excellent physicochemical properties<sup>[4]</sup> and a wide antimicrobial spectrum,<sup>[5]</sup> silver nanoparticles have become a promising material in the development of antimicrobial alternatives and are widely utilized in wound dressings. Compared to Ag nanoparticles,  $\text{Ag}^+$  exhibits enhanced antimicrobial activity because Ag nanoparticles present bactericidal activity through oxidation to  $\text{Ag}^+$ ,<sup>[6]</sup> which is a slow process and leads to low effective silver concentrations.<sup>[7]</sup> However, the  $\text{Ag}^+$  is ultimately consumed, and the antibacterial activity can be maintained for only a period of time. Thus, wound dressings that can load  $\text{Ag}^+$  and extend drug release are highly desirable. One potential set of materials for these dressings is hydrogels because of their softness similar to those of extracellular matrixes and adjustable physicochemical properties.<sup>[8]</sup> Moreover, hydrogels can

form physical barriers at bleeding sites to aid in hemostasis, maintain a moist wound environment, and allow oxygen to permeate.<sup>[2a,9]</sup> In addition, since pH and temperature play vital roles in the wound healing process, one essential aspect of desirable wound dressings lies in being pH-responsive and temperature-responsive.

Agarose, a neutral polysaccharide extracted from marine algae,<sup>[10]</sup> can form a stable thermoreversible gel via physical cross-linking without a cross-linking agent.<sup>[11]</sup> Because of its ideal biocompatibility, unique mechanical properties, and excellent gelling properties,<sup>[11c,12]</sup> agarose has attracted increasing attention and is widely used in the biomedical field for drug delivery,<sup>[13]</sup> cell therapy,<sup>[14]</sup> and tissue engineering.<sup>[15]</sup> However, its relatively low degree of chemical complexity limits the direct application of agarose to many delicate chemical and biological reactions.<sup>[11c]</sup> Introducing functional groups to agarose is an effective way to modify its physicochemical properties. Carboxymethyl modification can effectively improve the surface properties of hydrogels and promote cell proliferation. Moreover, the carboxymethyl group is an active group that can readily react with other chemicals, thus introducing new functions to the materials.


Herein, we designed a novel macroporous hydrogel dressing with antibacterial and anti-inflammatory capabilities for accelerated wound healing. Carboxymethyl agarose, a biocompatible

## 1. Introduction

Chronic wounds resulting from bacterial infection have become a main medical threat and challenge,<sup>[1]</sup> as bacteria can compete with the immune system and subsequently invade viable tissue,<sup>[2]</sup> especially for *Staphylococcus aureus*-associated skin wound infections, which usually result in serious tissue damage.<sup>[3]</sup> On the other hand, although inflammation is a critical phase of the wound healing process, long-lasting inflammation may still cause tissue damage and delay wound healing. Thus, the demands for wound dressings with antibacterial and anti-inflammatory properties are urgent.

Prof. W.-C. Huang, R. Ying, W. Wang, Y. Guo, Y. He, X. Mo, Prof. C. Xue, Prof. X. Mao  
College of Food Science and Engineering  
Ocean University of China  
Qingdao 266003, China  
E-mail: xuech@ouc.edu.cn; xzhmao@ouc.edu.cn

Prof. C. Xue, Prof. X. Mao  
Laboratory for Marine Drugs and Bioproducts  
Qingdao National Laboratory for Marine Science and Technology  
Qingdao 266237, China

 The ORCID identification number(s) for the author(s) of this article can be found under <https://doi.org/10.1002/adfm.202000644>.

DOI: 10.1002/adfm.202000644

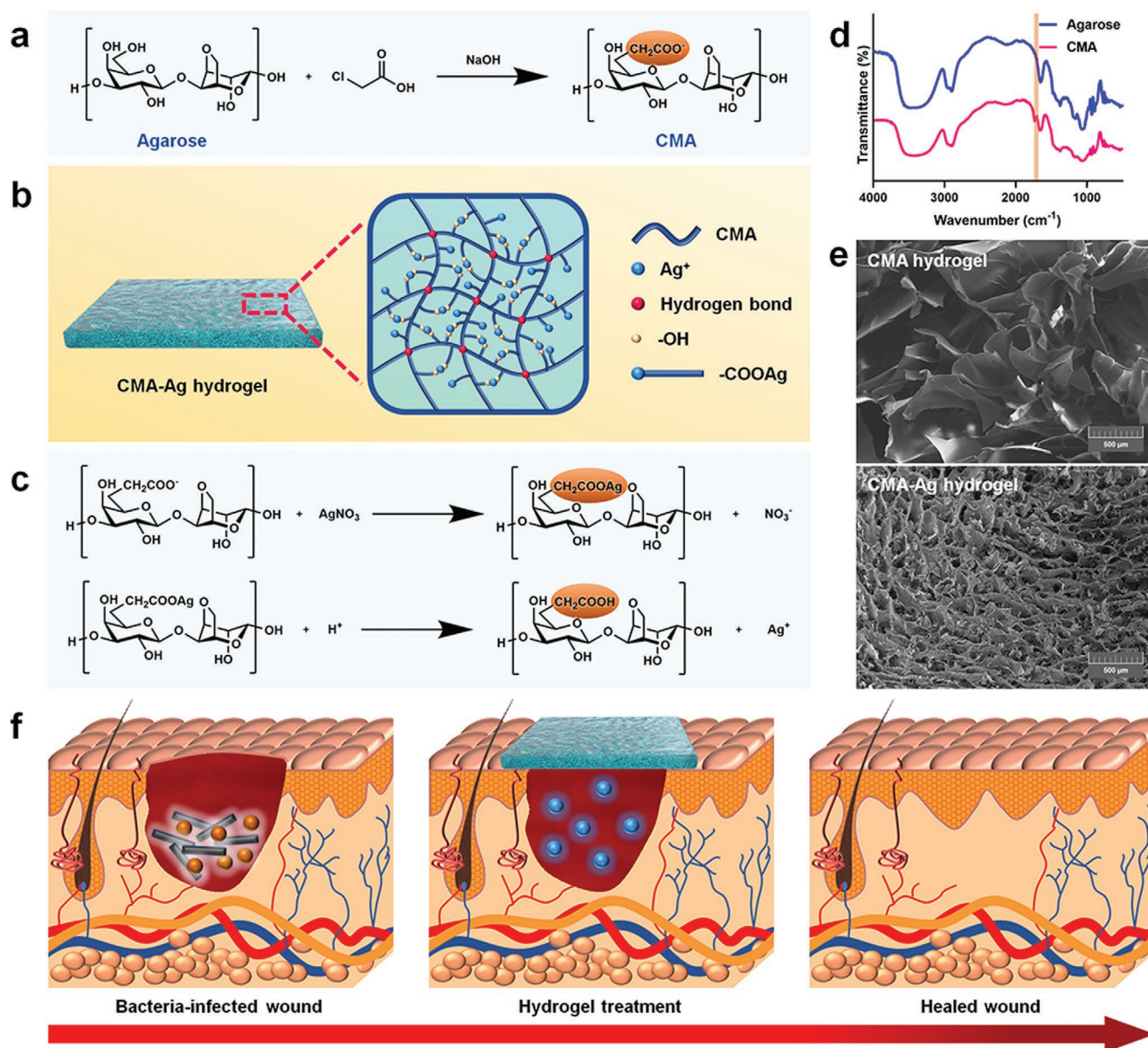


**Figure 1.** Schematics and architecture of the a) CMA molecule and b) CMA-Ag hydrogel. c) The pH-responsive release of Ag<sup>+</sup> from the CMA-Ag hydrogel. Structural and morphological characterization: d) FT-IR spectra of the agarose and CMA molecules and e) SEM images of the CMA and CMA-Ag hydrogels. f) Application of the CMA-Ag hydrogel to wound healing.

polymer, was prepared from agarose. The hydrogel matrix was formed by hydrogen bonding and supramolecular complexation. The morphology, antibacterial properties, biocompatibility, pH-responsiveness, temperature-responsiveness, and wound healing properties of the hydrogel dressing were evaluated.

## 2. Results and Discussions

### 2.1. Synthesis of CMA and Preparation of CMA-Ag Hydrogel

Synthesis of CMA and gelation mechanism of the hydrogel is illustrated in **Figure 1**. The FT-IR spectra of CMA exhibit an absorption peak at 1708 cm<sup>-1</sup> that corresponds to the

carboxymethyl group (**Figure 1d**). This result confirms that CMA was successfully prepared. The hydrogel is obtained via hydrogen bonding and supramolecular complexation. In this hydrogel matrix, the CMA molecular chains are cross-linked by hydrogen bonding to form a supramolecular hydrogel, and the carboxymethyl groups on the CMA molecular chain are deprotonated and ionically interact with Ag<sup>+</sup> (**Figure 1c**). Meanwhile, the hydroxy groups in the CMA chains coordinate with Ag<sup>+</sup> to promote hydrogel formation. These interactions collectively act to provide the unique physicochemical properties of the CMA-Ag hydrogel. The effect of Ag<sup>+</sup> cross-linking on the morphology of the hydrogels was examined by SEM (**Figure 1e**). The SEM analysis reveals that the surface morphologies and porous structures of the CMA hydrogel and CMA-Ag hydrogel

are significantly different. Compared with the CMA hydrogel, the porous structure of the CMA–Ag hydrogel is more compact, and the pore size is smaller. This result can be attributed to the interwoven networks coordinated between CMA and the Ag<sup>+</sup> ions, which can reduce the space between the CMA polymer chains. The inherent interconnected porous structure of the hydrogels can remarkably enhance wound healing, as the characteristic porous structure allows blood and tissue exudates to be rapidly absorbed into the hydrogels.<sup>[16]</sup>

Ultraviolet–visible (UV–vis) absorption spectra were recorded to further investigate the gelation mechanism of the CMA–Ag hydrogel (Figure S1, Supporting Information). The absorbance intensity increases significantly with increasing Ag<sup>+</sup> ion concentration, with the maximum absorption band undergoes a redshift that corresponds to the coordination of the Ag<sup>+</sup> ions with empty orbitals to the CMA molecules with abundant hydroxy groups. These results are in accordance with the SEM images of the CMA and CMA–Ag hydrogels (Figure 1e) and suggest that the rapid hydrogel matrix formation can be attributed to cross-linking by the Ag<sup>+</sup> ions, which form complexes with the hydroxy groups in the CMA molecules.

## 2.2. In Vitro Investigation of Cytocompatibility and Hemocompatibility

Biocompatibility is the primary concern for the in vivo biomedical application of a hydrogel. To initially investigate the

biocompatibility of the hydrogels, the cytocompatibility and hemocompatibility of CMA and CMA–Ag hydrogels were tested. The cytocompatibility was evaluated using a live/dead assay. As shown in Figure 2a, the fluorescence images reveal that all of the hydrogels are cytocompatible, since a large number of live cells are observed on the surface of the hydrogels after 3 d of culture, and the cell viability in all of the hydrogels increases with increasing culture time (Figure 2b), indicating the lack of cytotoxicity toward fibroblast cells. The cytocompatibility of the hydrogels was further evaluated by a standard 3-(4,5-dimethylthiazol-2-yl)-2,5-diphenyltetrazolium bromide (MTT) assay. As presented in Figure 2c, no significant cytotoxicity is observed in response to the gel extracts. More than 95% of the cells are viable even at the highest Ag<sup>+</sup> concentration (CMA–Ag-H) of the dilute hydrogel solution presented. These results suggest that the CMA–Ag hydrogel can be used in biological applications without causing long-term effects on biological growth. The blood compatibility of the hydrogels was investigated by a hemolysis assay, and no obvious hemolysis is observed (Figure 2d,e). These results demonstrated that the CMA and CMA–Ag hydrogels have excellent cytocompatibility and hemocompatibility.

## 2.3. Swelling of the Hydrogels

Swelling is an essential property of hydrogels. To investigate the swelling dependence on pH, the reversible swelling-shrinking

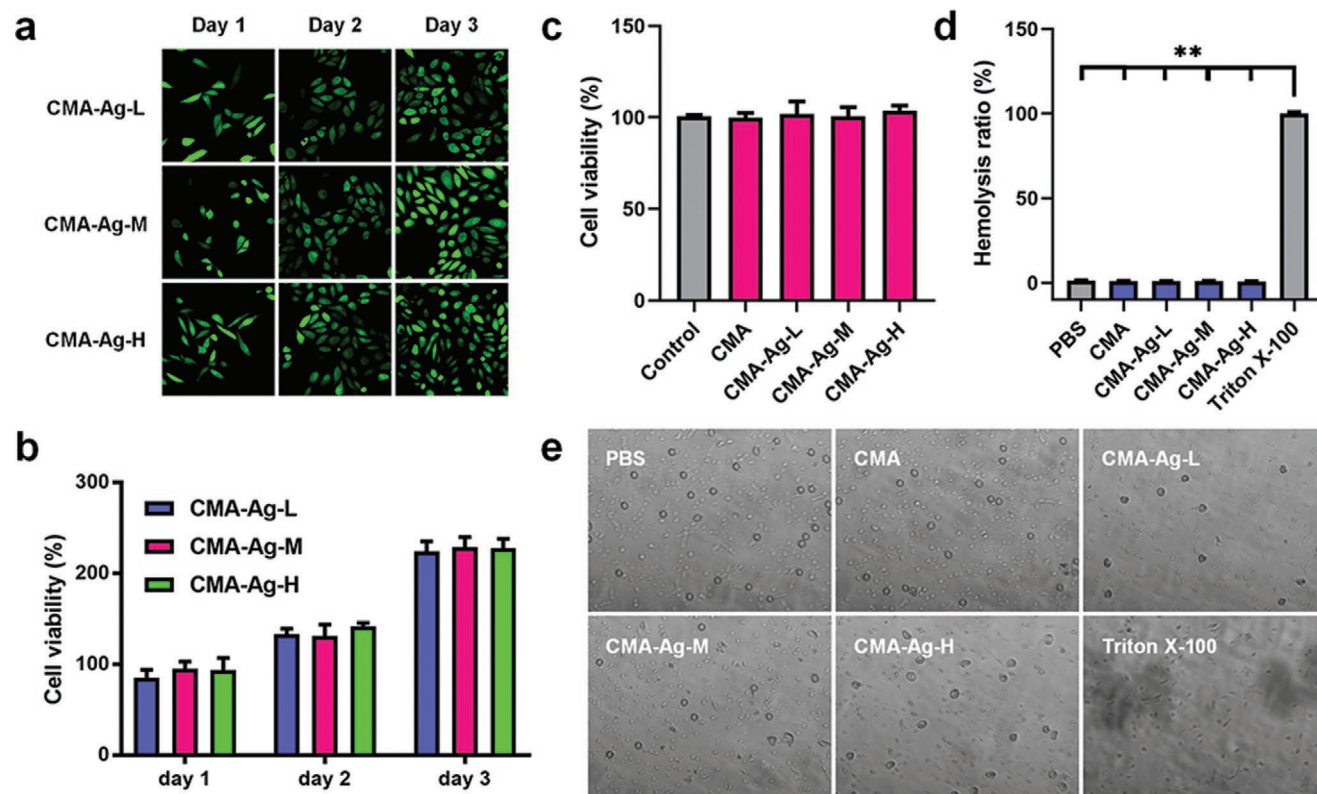


**Figure 2.** Cytocompatibility and hemocompatibility analysis. a) Live/dead staining fluorescent images, b) statistical data from the live/dead assay, c) statistical data from the MTT assay, d) statistical data from the hemolysis assay, and e) micrographs of the hemolysis assay. \* $p < 0.05$  and \*\* $p < 0.01$ .

behavior of hydrogels was measured at pH 7.4 and 2.0. As presented in Figure S2 (Supporting Information), all of the CMA–Ag hydrogels, independent of the  $\text{Ag}^+$  content, show a constant pH response between the shrunken (pH 7.4) and swollen states (pH 2.0) over three subsequent cycles. Generally, hydrogels composed of polyacidic polymers tend to swell more at basic pH because of the charge repulsion between the polymer chains caused by deprotonation.<sup>[13,17]</sup> In addition, acidic conditions increase protonation of the CMA, thus increasing the intermolecular hydrogen bonding between CMA chains and resulting in shrinkage of the hydrogels. However, the CMA–Ag hydrogel, which is cross-linked by  $\text{Ag}^+$  ions that form complexes with the hydroxy groups in the CMA molecular chains, swells more at acidic pH because acidic conditions are likely to disrupt the complexation between  $\text{Ag}^+$  ions and hydroxy groups. The loss of the complexation can be offset somewhat by the hydrogen bonding, but overall, there is a decrease in the strength of the intermolecular interactions under acidic conditions, leading to swelling of the hydrogel.

#### 2.4. Release of Silver Ions

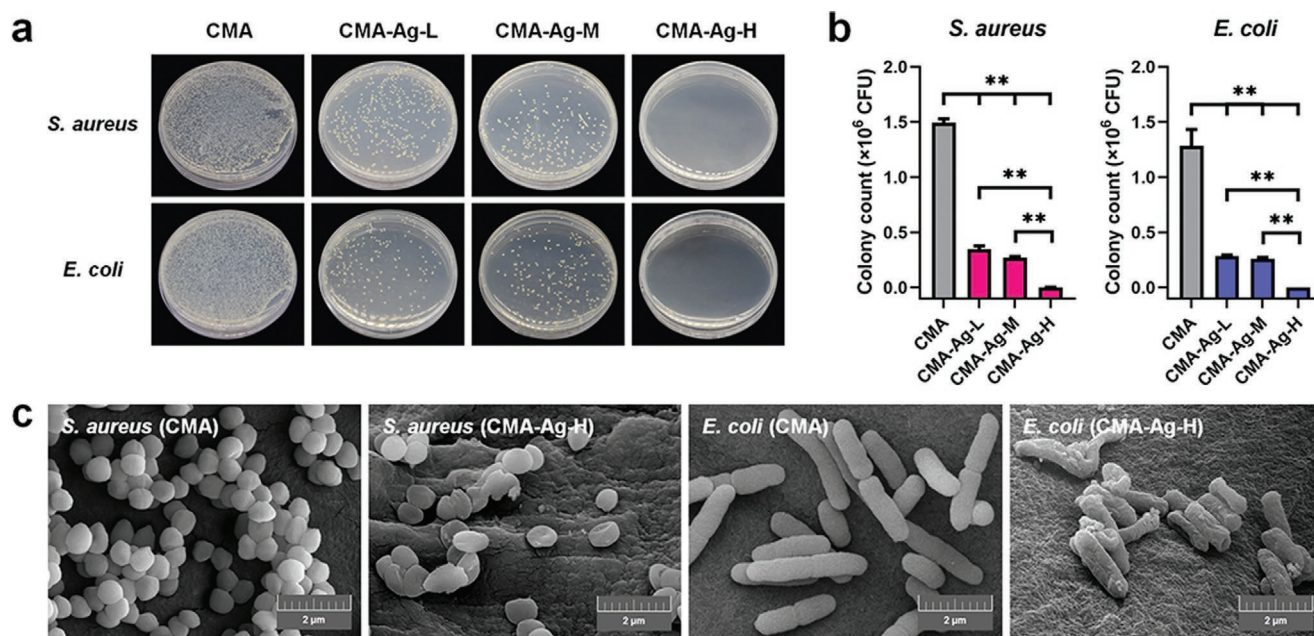
The in vitro release of  $\text{Ag}^+$  from the hydrogels was investigated at pH 2.0, 5.6, and 7.4, and the cumulative amount of release (%) was measured at various time points. The pH level is the key parameter of wound healing, and the pH of the wound environment can vary significantly depending on the type of wound and the stage of the healing process.<sup>[18]</sup> During the healing phase, the pH of the wound environment is acidic, ranging from pH 5.0 to 6.5.<sup>[18]</sup> As presented in Figure S3 (Supporting Information),  $\text{Ag}^+$  ions are released from the CMA–Ag hydrogels in a controlled manner over a prolonged period of

time. At all measurement time points, the release of  $\text{Ag}^+$  increases with decreasing pH. This occurs because for the hydrogels under higher pH, the ionic interaction between  $\text{Ag}^+$  and deprotonated CMA molecules contributes to the retention of  $\text{Ag}^+$  in the hydrogels and prevents  $\text{Ag}^+$  release, whereas lower pH leads to the disruption of ionic interaction and release of  $\text{Ag}^+$  (Figure 1c). Interestingly, the amounts of released  $\text{Ag}^+$  per unit time are similar in all the CMA–Ag hydrogels with different  $\text{Ag}^+$  contents.

The activities of cells and enzymes around wounds change at different temperatures. Thus, temperature is an important aspect of the wound healing process. To test the temperature-responsiveness of the CMA–Ag hydrogels, the in vitro release of  $\text{Ag}^+$  ions from CMA–Ag hydrogels was studied at 4 °C, 20 °C, and 37 °C, and the cumulative amount of release (%) was measured at various time points. As shown in Figure S4 (Supporting Information), at all measurement time points, the release of  $\text{Ag}^+$  increases with increasing temperature. This occurs because for the CMA–Ag hydrogels, which are cross-linked by complexation between  $\text{Ag}^+$  ions and hydroxy groups, higher temperatures are likely to disrupt the complexation, leading to release of  $\text{Ag}^+$ .

#### 2.5. In Vitro Antibacterial Activity of the CMA–Ag Hydrogel

The antibacterial ability of the hydrogels was evaluated in vitro against two bacterial strains, *S. aureus* and *Escherichia coli*, which are responsible for most infections.<sup>[2b]</sup> As shown in Figure 3a,b, the CMA hydrogel exhibits no obvious antibacterial behavior. In contrast, after contact with CMA–Ag–H, all of the *S. aureus* and *E. coli* are killed. CMA–Ag–L and CMA–Ag–M show 23% and 12% survival ratios for *S. aureus* and 22% and 20% survival ratios for *E. coli*, respectively. The hydrogels



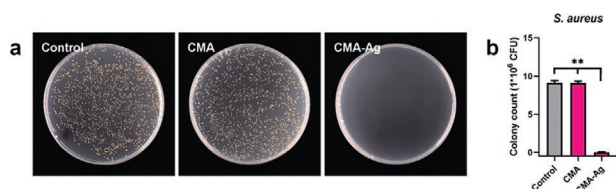
**Figure 3.** In vitro antibacterial activities of the CMA–Ag hydrogels against *S. aureus* and *E. coli*. a) Photographs of agar plates and b) corresponding statistical data of colonies of *S. aureus* and *E. coli*. c) SEM images showing the morphological changes of *S. aureus* and *E. coli* after incubation with CMA and CMA–Ag–H hydrogels. \* $p < 0.05$  and \*\* $p < 0.01$ .

exhibit obvious antibacterial activity in the presence of Ag<sup>+</sup>, and the CMA–Ag–H hydrogel with the highest Ag<sup>+</sup> content exhibits the best antibacterial effects against both *S. aureus* and *E. coli*. These results indicate that the antibacterial properties of the samples can be attributed to the Ag<sup>+</sup> released from the hydrogels, and the antibacterial effect increases with increasing Ag<sup>+</sup> content.

To understand the antibacterial process of the CMA–Ag hydrogel, the cell membrane integrity as well as the morphology of the bacteria on the hydrogels were observed by SEM (Figure 3c). After contact with the CMA–Ag–H hydrogel, significant morphological changes and damage are observed on the bacteria. The surface of the bacteria is wrinkled, distorted, and no longer intact. Furthermore, condensed *S. aureus* and shrunken *E. coli* are observed. In contrast, bacteria treated with CMA hydrogel present regular cellular morphology with a smooth surface. Compared to the CMA hydrogel, only a small amount of bacteria attaches to the surface of the CMA–Ag–H hydrogel, indicating that the CMA–Ag hydrogel can prevent bacterial adherence and biofilm formation. These results are consistent with the antibacterial mechanism of Ag<sup>+</sup> ions that Ag<sup>+</sup> ions can induce the destruction of the bacterial membrane.<sup>[19]</sup>

## 2.6. In Vivo Antibacterial Activity of the CMA–Ag Hydrogel

To investigate the antibacterial activity of the CMA–Ag hydrogel in vivo, the bacteria from the infected tissues were cultured after 2 d of treatment. The culture derived from infected tissues suggests that the wounds from the control and CMA groups show high bacterial growth, while the CMA–Ag–H hydrogel presents strong antibacterial activity against *S. aureus* (Figure 4). These results indicate that the CMA–Ag hydrogel



**Figure 4.** In vivo antibacterial activity against *S. aureus* infection. a) Photographs of *S. aureus* colonies growing on LB agar plates derived from tissues from different groups and b) the statistical data of *S. aureus* colonies from different groups. \* $p < 0.05$  and \*\* $p < 0.01$ .

has strong antibacterial activity in vivo and further confirm that the antibacterial properties of the CMA–Ag hydrogel originate from Ag<sup>+</sup> ions.

## 2.7. In Vivo Evaluation of Wound Healing

A cutaneous wound model was applied to assess the wound repair efficacy of the CMA–Ag hydrogel. The wound healing process was monitored photographically after treatments (Figure 5a). The CMA–Ag hydrogel markedly accelerates wound closure compared to both the control and CMA groups. Differences in wound size between the control and CMA–Ag groups start to appear after treatment for 4 d, and significant wound closure is observed in the CMA–Ag group compared to the control and CMA groups on day 8. After 14 d of treatment, the wounds treated with CMA–Ag hydrogel exhibit no open wounds and become smooth with new epidermal tissue, while 30% and 14% of wounds remain open with uneven scars in the control and CMA groups, respectively (Figure 5b). The results suggest that the hydrogel with embedded Ag<sup>+</sup> ions accelerates wound closure and skin regeneration. The calculation of

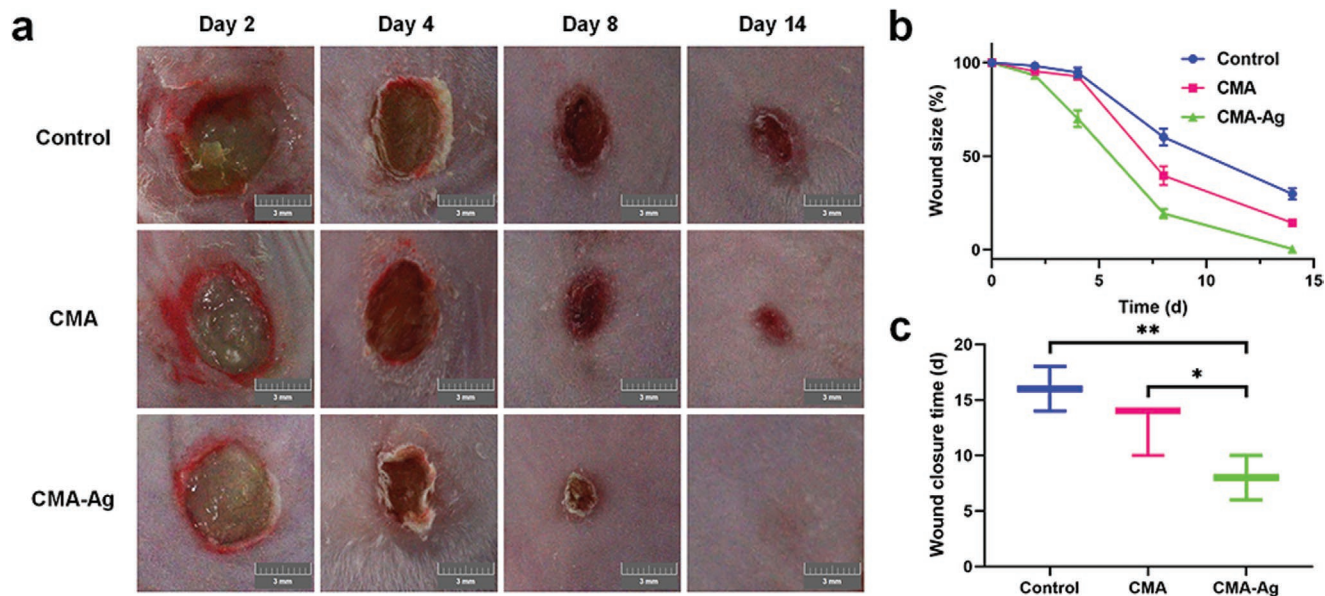


**Figure 5.** In vivo wound healing evaluation. a) Photographs of *S. aureus*-infected wounds of different groups on days 2, 4, 8, and 14. b) Changes in wound size for different groups. c) Wound closure times for different groups. \* $p < 0.05$  and \*\* $p < 0.01$ .

wound size and wound closure time further confirms that the CMA–Ag group demonstrates the best wound healing efficacy compared to the other groups (Figure 5b,c).

Wound healing was further assessed using histological examination. Tissues from the control, CMA, and CMA–Ag groups were stained with hematoxylin and eosin (H&E) on days 2, 4, 8, and 14 (Figures 6, 7, and S5, Supporting Information). On day 2, attenuated dermis tissue, damaged collagen fibers, and cell debris are observed in all three groups. Additionally, a large number of neutrophils appear in all three groups, indicating a serious infection by *S. aureus*. On day 4, dermal fibroblasts and new blood vessels are observed in the CMA and CMA–Ag groups. Additionally, a large number of red blood cells are observed in the CMA–Ag group. On day 8, regenerated dermal tissue with new skin appendages, such as hair follicles, is observed in the CMA–Ag group. However, many neutrophils appear, and the epidermis becomes thick in the control and CMA groups. On day 14, almost complete regeneration of dermis tissue with skin appendages such as hair follicles is observed in the CMA–Ag group, and the epidermis and dermis tissues of the CMA–Ag group are almost the same as those of normal skin, indicating better regeneration. In comparison, the control and CMA groups do not show complete regeneration of epidermal and dermal tissue. Thick epidermis and dead cell debris are observed in the control and CMA groups. Furthermore, necrotic foci and a large number of white blood cells, especially neutrophils, appear in the control and CMA groups, indicating that the wounds have not yet healed.

Masson's trichrome staining was applied to depict the deposition and organization of collagen fibers in the wound healing process (Figure 8a and 7c). As presented in Figure 8a, increased collagen deposition in the wound region is observed in all three groups. However, the collagen deposition is denser and more organized in the CMA–Ag group. On day 14, mature collagen fibers are observed in the CMA–Ag group. On the other hand, the collagen fibers of the control and CMA groups are still partially dysplastic.

In addition, histological analysis of the major organs (heart, liver, spleen, lungs, and kidneys) in each group presents integrated tissue structure without abnormal defects or damage after 14 d of treatment (Figure 8b), indicating that the CMA–Ag hydrogel can be a safe therapeutic material for wound healing.

The accelerated wound healing is probably due to the broad-spectrum antibacterial ability and excellent physicochemical properties of the CMA–Ag hydrogel. The porous structure of the hydrogel could absorb the tissue exudate. The carboxymethyl modification of agarose probably improves the surface properties of the hydrogel and promotes cell proliferation. The broad-spectrum antibacterial capacity and excellent physicochemical properties of the CMA–Ag hydrogel protect the wound from further injury and bacterial infections, which often occur during the wound healing process. Considering that the CMA–Ag hydrogel is able to sustainably release  $\text{Ag}^+$  ions, the hydrogel can continuously protect wounds from bacterial infection. In addition, the hydrogel can maintain a moist environment for tissue formation. Inflammation is an essential part of the wound healing process by which white blood cells protect wounds from infection. However, long-lasting inflammation

can result in delayed wound healing and even tissue damage. On day 4, a large number of white blood cells are observed in the CMA–Ag group. However, on day 8, the number of white blood cells in the CMA–Ag group is significantly reduced compared to the other groups. This occurs because  $\text{Ag}^+$  released from the CMA–Ag hydrogel stimulates immune functions to produce a large number of white blood cells in the early phase of the wound healing process, leading to synergistic antibacterial activity, and then quickly reduces the number of white blood cells so that inflammation occurs for a shorter amount of time than in normal processes, minimizing the tissue damage caused by inflammation. As a result, benefiting from less bacterial infection, the inflammatory reaction of the CMA–Ag group is more moderate than that of the other groups.

### 3. Conclusion

In summary, we present a novel macroporous hydrogel dressing for bacteria-associated wound management. The hydrogel was shown to exhibit pH-responsiveness and temperature-responsiveness and to release  $\text{Ag}^+$  steadily over a prolonged period of time. By taking advantage of  $\text{Ag}^+$ , this hydrogel composite exhibited significant antibacterial activity both in vitro and in vivo and significantly accelerated skin regeneration and wound healing processes while retaining excellent cytocompatibility and hemocompatibility. Moreover, the hydrogel could cause the inflammation process to occur earlier and for a shorter amount of time than in a normal process, effectively reducing the tissue damage caused by inflammation. Overall, the hydrogel could be a good alternative to current wound dressings and has great potential in the field of clinical treatment of wound infection.

### 4. Experimental Section

**Synthesis of Carboxymethyl Agarose:** The agarose (5 g) was suspended in 2-propanol (50 mL) at room temperature under stirring for 30 min. Then, a NaOH solution (1.33 M, 50 mL) and chloroacetic acid (2.5 g) were added to the suspension, which was stirred for 30 min. The resulting suspensions were heated for 2 h at 70 °C, followed by filtration, washing with ethanol solution, drying, and storage at 4 °C for further use.

**Preparation of Hydrogels:** CMA was dissolved in distilled water at 70 °C.  $\text{AgNO}_3$  (0.1 M) was then added to the carboxymethyl agarose solutions (2% w/v) to provide final  $\text{AgNO}_3$  concentrations of  $0.5 \times 10^{-3}$ ,  $1 \times 10^{-3}$ , and  $2 \times 10^{-3}$  M, and the mixtures were stirred for 10 min before being cooled at 4 °C to obtain carboxymethyl agarose-silver ion (CMA–Ag) composite hydrogels of CMA–Ag–L ( $0.5 \times 10^{-3}$  M), CMA–Ag–M ( $1 \times 10^{-3}$  M), and CMA–Ag–H ( $2 \times 10^{-3}$  M), respectively. A control CMA hydrogel was prepared without  $\text{AgNO}_3$ .

**Characterization:** The chemical structure of the samples was confirmed by Fourier transformation infrared (FT-IR) spectra. The FT-IR spectra of the samples were recorded in the range of 4000–500  $\text{cm}^{-1}$  using an FT-IR spectrometer (Thermo Scientific Nicolet iS10). The UV–vis spectra were recorded on a microplate reader (Perlong Medical DNM-9602). The hydrogel microstructures were characterized using a scanning electron microscope (SEM; Quanta FEG250) at an acceleration voltage of 10 kV. Prior to imaging, all the samples were mounted on aluminum stubs using conductive carbon tape, and then the samples were sputter-coated with a platinum film.

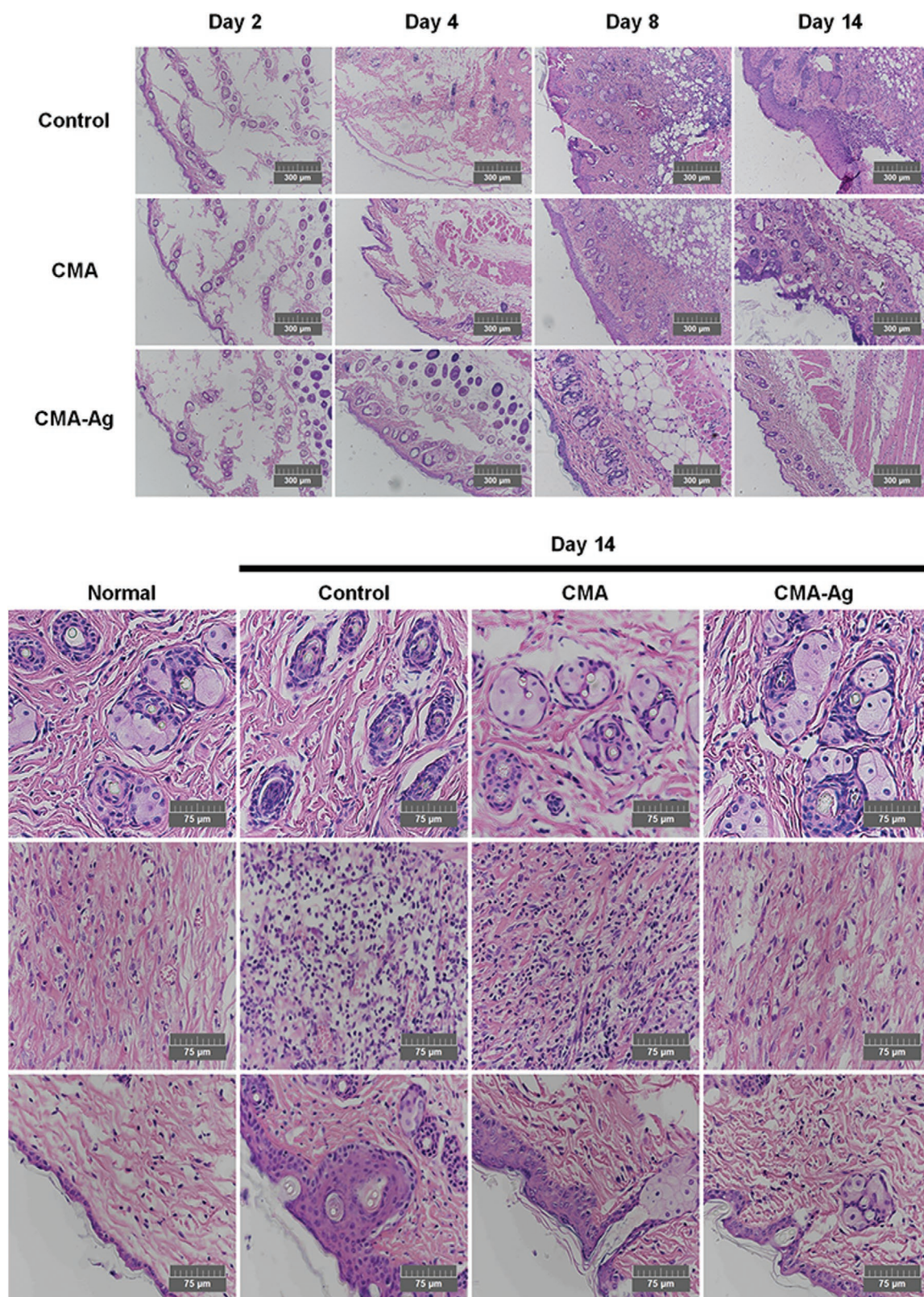


**Figure 6.** Micrographs of H&E stained tissue slices from different groups on days 2, 4, 8, and 14.

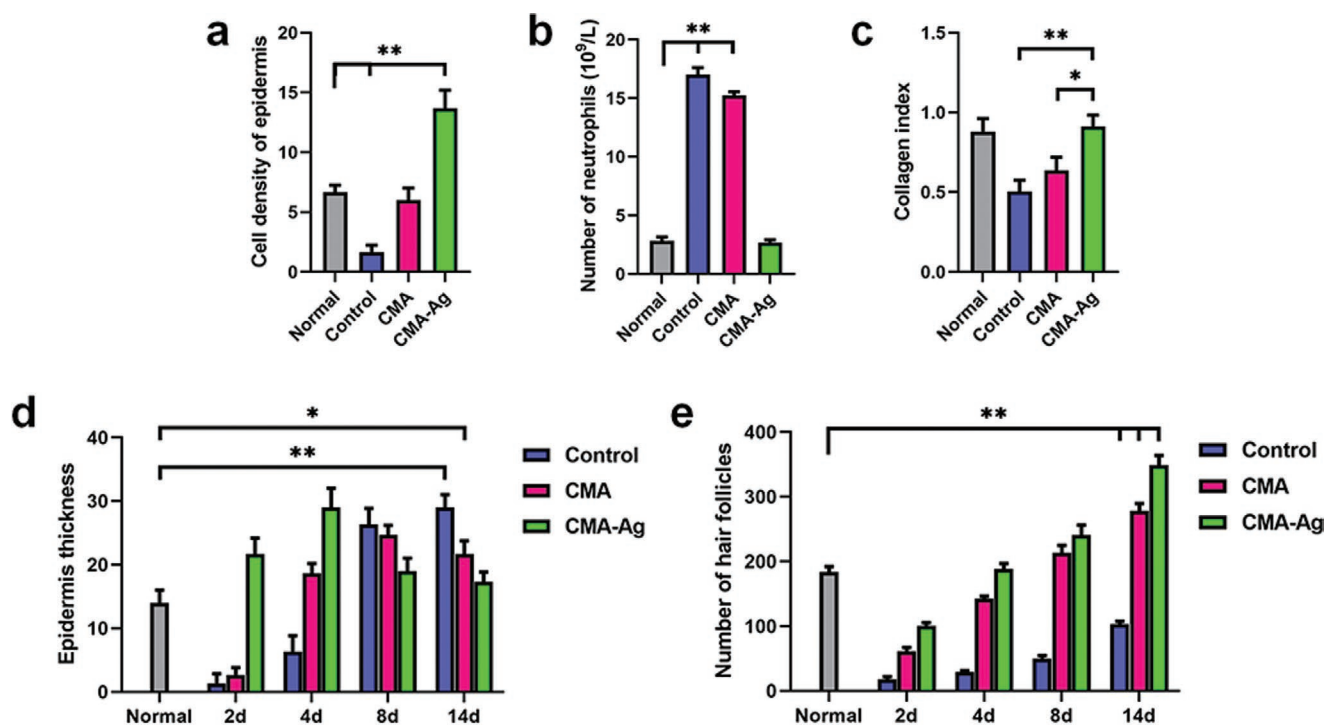


**Figure 7.** Wound healing statistical data of different groups after 14 d of treatment. a) Cell density of epidermis, b) number of neutrophils, c) collagen index, d) epidermis thickness, and e) number of hair follicles. \* $p < 0.05$  and \*\* $p < 0.01$ .

**Cytocompatibility and Hemocompatibility Investigation:** The *in vitro* cytocompatibility of the hydrogels was investigated via live/dead assay and MTT [3-(4,5-dimethylthiazol-2-yl)-2,5-diphenyltetrazolium bromide] assay. The hemocompatibility of the hydrogels was investigated using a hemolysis assay.

**Swelling Tests:** Swelling tests were performed in aqueous solutions at various pH values that were adjusted using HCl (0.5 M) or NaOH (0.5 M) at room temperature. The masses of the dried ( $m_{dry}$ ) and swollen ( $m_{swollen}$ ) hydrogels were measured. The swelling degree was calculated as follows

$$\text{Swelling degree (\%)} = \frac{(m_{swollen} - m_{dry})}{m_{dry}} \times 100\% \quad (1)$$

**In Vitro Release Studies:** The release of  $Ag^+$  from the hydrogels was determined in PBS. The samples were immersed in PBS (30 mL) at various pH levels and temperatures. The amount of  $Ag^+$  released into the medium was determined by inductively coupled plasma mass spectrometry (ICP-MS, Agilent 7700s) at various time points. All the experiments were conducted in triplicate.

**In Vitro Antibacterial Activity Assays:** The antibacterial activity of the hydrogels was evaluated by the spread plate method with *S. aureus* (Gram-positive) and *E. coli* (Gram-negative) as bacterium models. The bacterial stock suspensions ( $1.0 \times 10^6$  CFU  $mL^{-1}$ ) and hydrogel samples were added to 96-well plates and incubated at 37 °C for 1 h. The solutions in each well were diluted 1000 times and uniformly plated onto LB agar plates and incubated for 24 h for *S. aureus* and 48 h for *E. coli* at 37 °C. Then, the number of CFUs on the LB agar plates was counted. The bacterial survival ratio was calculated as follows:

$$\text{Survival ratio (\%)} = \text{CFU}/\text{CFU}_0 \times 100\% \quad (2)$$

where CFU is the number of colony forming units with the hydrogels and  $CFU_0$  is the number of colony forming units without the hydrogels.

The morphologies of the CMA-Ag hydrogel-treated and CMA hydrogel-treated bacterial cells were examined using scanning electron

microscopy. Briefly, bacterial cells were incubated with hydrogels for 2 h. Then, the bacterial cells were fixed with 2.5% glutaraldehyde in sodium phosphate buffer (pH 7.4) for 1 h. Subsequently, the hydrogels with bacterial cells were rinsed with sodium phosphate buffer and dehydrated with a graded ethanol series. SEM images were taken at an acceleration voltage of 10 kV.

**In Vivo Wound Healing Assay:** Male BALB/c mice were randomized to three groups: the control group, CMA group, and CMA-Ag group. Namely, the control group had no further treatment, the CMA group was covered with CMA hydrogel dressing, and the CMA-Ag group was covered with CMA-Ag-H hydrogel dressing. The dorsal surface of the mouse was depilated under anesthesia. Two partial thickness wounds with a 5 mm diameter were made on the dorsum of each mouse. The dried CMA hydrogels were soaked with 200  $\mu L$  of *S. aureus* ( $1.0 \times 10^6$  CFU  $mL^{-1}$ ) for 1 h, and the wounds of the three groups were treated with soaked CMA hydrogels. The prepared CMA hydrogel and CMA-Ag-H hydrogel were directly applied to the wounds. Following surgery, the wound areas of the CMA and CMA-Ag groups were completely covered with hydrogel dressings and secured using Tegaderm (3M). The dressings were renewed every 2 d, and photographs of the wounds were taken on days 2, 4, 8, and 14 with a digital camera. The skin tissue samples were fixed with 10% formalin solution and embedded in paraffin to prepare the pathological slides. After hematoxylin and eosin (H&E) and Masson's trichrome staining of the samples, the histological images were observed by an optical microscope. Moreover, 3  $\mu L$  of the exudate from the wound was collected on day 2 and then diluted 200 times with LB broth. Subsequently, 20  $\mu L$  of each dilution was spread on LB agar plates and cultured at 37 °C for 8 h. The major organs, including the heart, liver, spleen, lungs, and kidneys, were harvested and stained with H&E for histological analysis. All of the animal care and experiments were reviewed and approved by the Animal Investigation Ethics Committee of Ocean University of China (No. SPXY20190905).

**Statistical Analysis:** All the data are presented as the mean value  $\pm$  standard deviation based on experiments performed in triplicate or



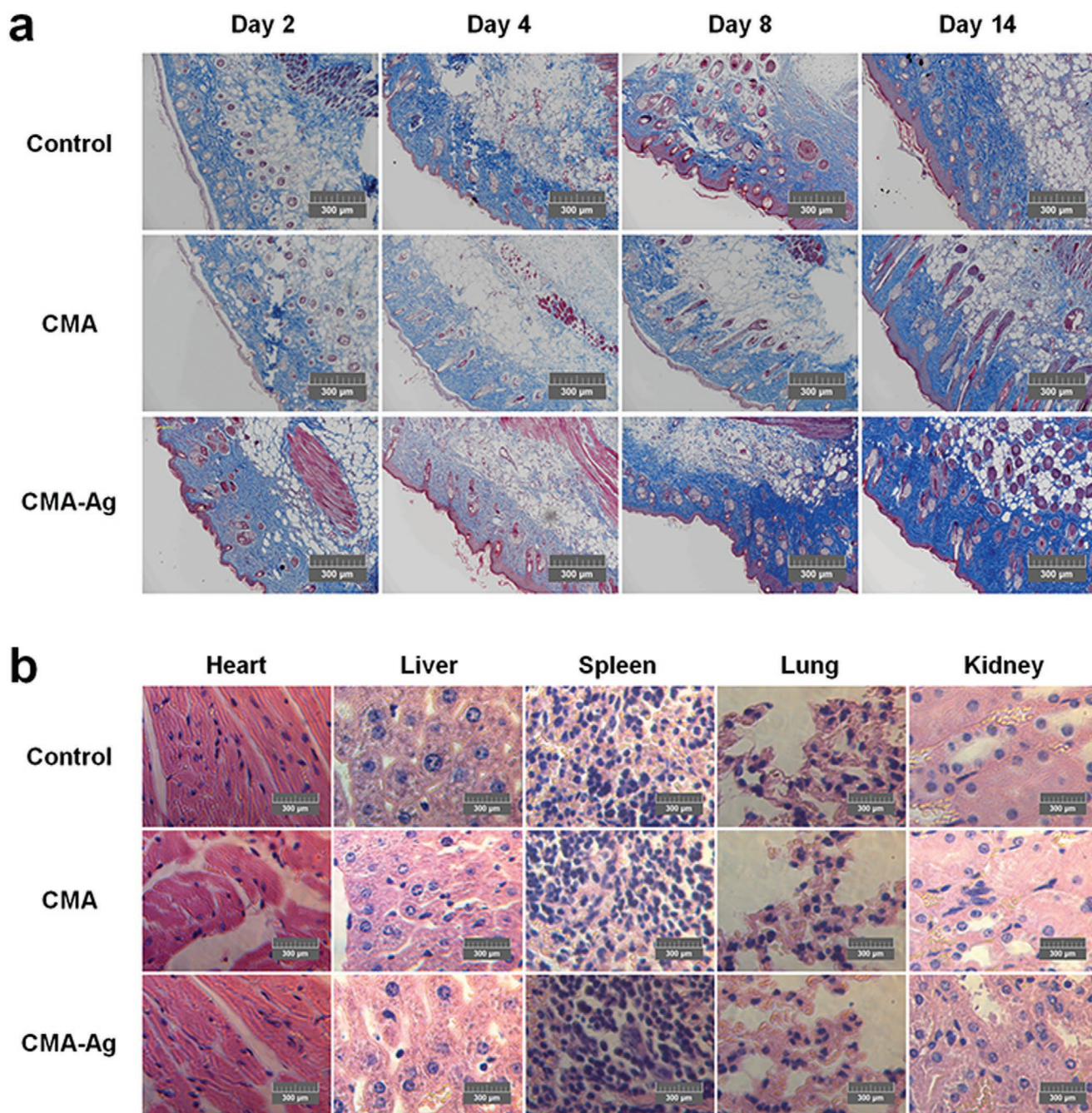


**Figure 8.** a) Micrographs of Masson's trichome-stained tissue slices from different groups on days 2, 4, 8, and 14. b) Micrographs of H&E-stained major organ tissue slices from different groups after 14 d of treatment.

more. Statistical significance was determined using one-way analysis of variance (ANOVA), and statistically significant differences are shown with  $*p < 0.05$ ,  $**p < 0.01$ .

## Supporting Information

Supporting Information is available from the Wiley Online Library or from the author.

## Acknowledgements

W.C.H. and R.Y. contributed equally to this work. This work was supported by the National Natural Science Foundation of China (31922072), China Agriculture Research System (CARS-48) and Taishan Scholar Project of Shandong Province (tsqn201812020).

## Conflict of Interest

The authors declare no conflict of interest.

## Keywords

agarose, antibacterial, biopolymers, hydrogels, wound healing

Received: January 22, 2020

Revised: February 27, 2020

Published online:

- [1] Q. Pang, D. Lou, S. Li, G. Wang, B. Qiao, S. Dong, L. Ma, C. Gao, Z. Wu, *Adv. Sci.* **2020**, *7*, 1902673.
- [2] a) J. Zhu, F. Li, X. Wang, J. Yu, D. Wu, *ACS Appl. Mater. Interfaces* **2018**, *10*, 13304; b) C. Mao, Y. Xiang, X. Liu, Z. Cui, X. Yang, K. W. K. Yeung, H. Pan, X. Wang, P. K. Chu, S. Wu, *ACS Nano* **2017**, *11*, 9010; c) Y. Zhang, P. Sun, L. Zhang, Z. Wang, F. Wang, K. Dong, Z. Liu, J. Ren, X. Qu, *Adv. Funct. Mater.* **2019**, *29*, 1808594; d) Y. Li, X. Liu, L. Tan, Z. Cui, X. Yang, Y. Zheng, K. W. K. Yeung, P. K. Chu, S. Wu, *Adv. Funct. Mater.* **2018**, *28*, 1800299; e) J. Zhou, A. L. Loftus, G. Mulley, A. T. A. Jenkins, *J. Am. Chem. Soc.* **2010**, *132*, 6566.
- [3] L.-j. Zhang, C. F. Guerrero-Juarez, T. Hata, S. P. Bapat, R. Ramos, M. V. Plikus, R. L. Gallo, *Science* **2015**, *347*, 67.
- [4] a) B. Le Ouay, F. Stellacci, *Nano Today* **2015**, *10*, 339; b) S. Shakya, Y. He, X. Ren, T. Guo, A. Maharjan, T. Luo, T. Wang, R. Dhakhwa, B. Regmi, H. Li, R. Gref, J. Zhang, *Small* **2019**, *15*, e1901065.
- [5] a) Z. Fan, B. Liu, J. Wang, S. Zhang, Q. Lin, P. Gong, L. Ma, S. Yang, *Adv. Funct. Mater.* **2014**, *24*, 3933; b) M. Wu, B. Ma, T. Pan, S. Chen, J. Sun, *Adv. Funct. Mater.* **2016**, *26*, 569.
- [6] K. Zheng, M. I. Setyawati, D. T. Leong, J. Xie, *Coord. Chem. Rev.* **2018**, *357*, 1.
- [7] S. Chernousova, M. Epple, *Angew. Chem., Int. Ed.* **2013**, *52*, 1636.
- [8] a) J. Li, D. J. Mooney, *Nat. Rev. Mater.* **2016**, *1*, 16071; b) C. Ghobril, M. W. Grinstaff, *Chem. Soc. Rev.* **2015**, *44*, 1820; c) L. Thai Minh Duy, D. Huu Thuy Trang, T. Thambi, V. H. G. Phan, J. H. Jeong, D. S. Lee, *Biomacromolecules* **2018**, *19*, 3536; d) R. Tian, X. Qin, P. Yuan, K. Lei, L. Wang, Y. Bai, S. Liu, X. Chen, *ACS Appl. Mater. Interfaces* **2018**, *10*, 17018.
- [9] a) G. Chen, Y. Yu, X. Wu, G. Wang, J. Ren, Y. Zhao, *Adv. Funct. Mater.* **2018**, *28*, 1801386; b) B. Saleh, H. K. Dhaliwal, R. Portillo-Lara, E. Shirzaei Sani, R. Abdi, M. M. Amiji, N. Annabi, *Small* **2019**, *15*, e1902232.
- [10] M. Li, D. Mitra, E.-T. Kang, T. Lau, E. Chiong, K. G. Neoh, *ACS Appl. Mater. Interfaces* **2017**, *9*, 1847.
- [11] a) T. Singh, T. J. Trivedi, A. Kumar, *Green Chem.* **2010**, *12*, 1029; b) T. A. Ulrich, A. Jain, K. Tanner, J. L. MacKay, S. Kumar, *Biomaterials* **2010**, *31*, 1875; c) Y. Su, B. Chu, Y. Gao, C. Wu, L. Zhang, P. Chen, X. Wang, S. Tang, *Carbohydr. Polym.* **2013**, *92*, 2245.
- [12] a) N. Jin, E. A. Morin, D. M. Henn, Y. Cao, J. W. Woodcock, S. Tang, W. He, B. Zhao, *Biomacromolecules* **2013**, *14*, 2713; b) T. J. Trivedi, D. Bhattacharjya, J.-S. Yu, A. Kumar, *ChemSusChem* **2015**, *8*, 3294.
- [13] N. Ninan, A. Forget, V. P. Shastri, N. H. Voelcker, A. Blencowe, *ACS Appl. Mater. Interfaces* **2016**, *8*, 28511.
- [14] S. Sakai, K. Kawabata, T. Ono, H. Ijima, K. Kawakami, *Biomaterials* **2005**, *26*, 4786.
- [15] Y. P. Singh, N. Bhardwaj, B. B. Mandal, *ACS Appl. Mater. Interfaces* **2016**, *8*, 21236.
- [16] J. Zhu, H. Han, F. Li, X. Wang, J. Yu, X. Qin, D. Wu, *Chem. Mater.* **2019**, *31*, 4436.
- [17] Q. Shi, H. Liu, D. Tang, Y. Li, X. Li, F. Xu, *NPG Asia Mater.* **2019**, *11*, 1.
- [18] a) R. Rahimi, M. Ochoa, A. Tarnayol, S. Khalili, A. Khademhosseini, B. Ziaie, *ACS Appl. Mater. Interfaces* **2017**, *9*, 9015; b) P. Mostafalu, A. Tamayol, R. Rahimi, M. Ochoa, A. Khalilpour, G. Kiaee, I. K. Yazdi, S. Bagherifard, M. R. Dokmeci, B. Ziaie, S. R. Sonkusale, A. Khademhosseini, *Small* **2018**, *14*, e1703509.
- [19] Q. Li, F. Lu, G. Zhou, K. Yu, B. Lu, Y. Xiao, F. Dai, D. Wu, G. Lan, *Biomacromolecules* **2017**, *18*, 3766.